Nuclear Materials and Energy 28 (2021) 101030

Contents lists available at ScienceDirect

Nuclear Materials and Energy

journal homepage: www.elsevier.com/locate/nme

SOLPS-ITER drift modelling of JET Ne and N-seeded H-modes

Elizaveta Kaveeva [a,*], Vladimir Rozhansky [a], Irina Veselova [a], Ilya Senichenkov [a], Carine Giroud [b], Richard A. Pitts [c], Sven Wiesen [d], Serguey Voskoboynikov [a]

[a] Peter the Great St. Petersburg Polytechnic University, Polytechnicheskaya 29, 195251 St. Petersburg, Russia
[b] CCFE, Culham Science Centre, Abingdon OX14 3DB, UK
[c] ITER Organization, Route de Vinon-sur-Verdon, CS 90 046, 13067 St Paul Lez Durance Cedex, France
[d] Forschungszentrum Jülich GmbH, Institut für Energie- und Klimaforschung – Plasmaphysik, D-52425 Jülich, Germany

ARTICLE INFO

Keywords:
SOLPS-ITER
JET modelling
Ne and N-seeding modeling

ABSTRACT

A numerical study is presented, using the SOLPS-ITER plasma boundary code with full drifts and currents activated, of impurity seeded JET discharges in support of high power H-mode experimental campaigns designed to compare two ITER candidate seeding species, nitrogen (N) and neon (Ne). Fluid-kinetic edge plasma simulations are first performed at lower levels of power into the scrape-off layer (SOL) and benchmarked against existing JET experimental data. Calculations are then performed for higher levels of SOL power to examine the impact of this key parameter on the efficiency of both radiators. From the code point of view, for the chosen JET parameters, Ne can be as efficient a divertor radiator as N at the same level of upstream separatrix $Z_{eff} < 1.5$ for moderate seeding, decreasing the peak power at outer target by factor ~ 3. Full detachment (state with the temperature below 5 eV along all the target) at the outer target can be obtained with both impurities at higher seeding, but in the case of Ne this leads to a higher Z_{eff} and significant radiation in the main SOL/pedestal. The indications from this JET code modelling, in comparison with previous similar simulations for ITER and ASDEX Upgrade with drifts turned on, are that there is a beneficial impact of machine size in improving impurity retention, substantiating the claim that both N and Ne will perform well as seed impurities for divertor power dissipation in ITER.

Introduction

One of the key issues of importance in the ITER Research Plan is the choice of extrinsic seed impurity for management of divertor power deposition [1]. Such seeding is mandatory on ITER during burning plasma (DT) operation. Of the two main candidate species, nitrogen (N) and neon (Ne), the latter is preferred on ITER from the point of view of avoiding plasma chemistry (principally the formation of tritiated ammonia during DT experiments [1]).

Plasma boundary modelling of ITER burning plasmas using the SOLPS-4.3 code (B2-EIRENE) without fluid drifts activated shows that both Ne and N should be equally effective as divertor radiators [1], due notably to the large scale size of the device. More recent simulations with the SOLPS-ITER (B2.5-EIRENE) code [2], for the moment considering only Ne, but including all drifts, also confirm efficient divertor power dissipation under partially detached conditions albeit with higher out-in target power flux asymmetries at lower degrees of detachment than in the absence of drifts. Here and further on in the paper the partially detached conditions are conditions when SOL flux tubes at scales comparable to energy flow width have temperature below 5 eV at the divertor target, and most part of energy flow coming through these tubes is dissipated.

Experimental H-mode seeding studies in JET and ASDEX Upgrade (AUG) with all-metal plasma-facing components (PFC) in the range of 18–26 MW of additional heating power have shown that, in general N, performs better than Ne, without strong degradation of confinement even with relatively strong degrees of detachment, associated with the majority of the radiative power dissipation occurring in the X-point region [3,4]. In the case of Ne, impurity transport and radiation in the pedestal tend to drive instabilities and stable H-modes are either not sustainable (AUG) [4] or confinement is strongly reduced (JET) [3]. In the latter case, the input power levels were insufficient in the experiments to maintain sufficient distance above the H-L back transition power for good confinement. It is for this reason that new experiments at

* Corresponding author.
E-mail address: kaveeva@spbau.ru (E. Kaveeva).

https://doi.org/10.1016/j.nme.2021.101030
Received 29 January 2021; Received in revised form 14 April 2021; Accepted 20 May 2021
Available online 5 June 2021

JET, with higher input power than was available for the study in [3] are important in the sense of allowing comparative studies between AUG and JET (differing by a factor of 2 in scale size) to be performed for the two ITER candidate divertor seeding species. Experiments and SOLPS-ITER modeling investigations of N/Ne seeded discharges have been also performed at DIII-D, a device with similar size of AUG but with carbon PFC. DIII-D results are in agreement with the findings at AUG that N is better retained in the divertor compared to Ne and that the inclusion of drifts and currents is necessary to interpret the experimental findings [5]. Numerical study of N-seeded JET H-modes was performed with code EDGE2D [6]. This modeling showed that at moderate power N is applicable radiator. Still it was done without drifts, which are shown to be significant contributors to divertor transport experimentally [7] and in modeling presented in this paper.

A similar SOLPS-ITER code study as that for ITER has been performed for AUG [8] (a device one third the ITER scale size), with focus on N seeding. Drifts are found to have a much stronger impact than in the case of the ITER simulations. In support of new experiments with increased input power, the same exercise has now been performed for JET, adding a third device, intermediate in size between AUG and ITER, to the modelling database. The results are reported here. Importantly, all three of these machines feature all-metal PFCs and vertical divertor target configurations, the latter largely eliminating differences in detachment thresholds due to geometry.

The JET simulations use the same approach as for the AUG and ITER modelling: profiles of cross-field transport coefficients are chosen to produce an H-mode transport barrier inside the separatrix, and, in the case of AUG and JET, to reproduce experimental Thomson scattering profiles at the outer midplane and Langmuir probe measurements at the outer target. This "numerical experiment" is designed as a predictive modelling exercise, in which the behavior at high values of power into the scrape-off layer (SOL), P_{SOL} is examined on the basis of simulations guided by previously published experimental data from N and Ne seeding experiments in JET at lower P_{SOL}.

Section "Simulation results", Section ""Calibration" exercise at moderate input power and trace impurity" describes general modeling setup and simulation for existing moderate power discharge with comparison to experimenal results, analysis of drift effects, and trace impurity distribution. Section "Simulation results", Section "Modelling results for high input power" describes the predictive modeling at bigger power input with N and Ne seeding ramp-up up to transition to full detachment of outer target. Conclusions are given in Section "Conclusions".

Simulation results

"Calibration" exercise at moderate input power and trace impurity

Experimental JET data from the study published in [3,9] are used to provide a "low P_{SOL}" benchmark for the SOLPS-ITER modelling at a fixed single D and low impurity concentration. The high triangularity (ITER-like) pulse number #85278 has input power of ~ 21 MW with power crossing the separatrix ~ 11 MW in inter ELM period, plasma current I_p = 2.5 MA and toroidal field B_T = 2.7 T [9] (cf. 0.8 MA/2.5 T for the AUG case studied in [8] and 15 MA/5.3 T on ITER). The power loss in the core was calculated using the bolometric reconstruction of radiated power outside the region modelled by SOLPS-ITER. It is a non-seeded discharge, but with low residual nitrogen concentration resulting from previous N-seeding discharges executed in the same experimental session. Section "Modelling results for high input power" will describe the results of predictive simulations at higher P_{SOL} in which scans of impurity seeding rate are made.

The full EIRENE model was used, accounting for neutral–neutral collisions. Two choices of sub-divertor modelling geometries were applied (see Fig. 1). The first is a full description (Fig. 1(a), left) of the (complex) sub-divertor volume filled with neutral gas previously used in JET SOLPS-ITER modelling to allow simulations of the neutral pressure at the pressure gauges located far below the sub-divertor [10]. The second (Fig. 1(a), right) is a simplified model in which some structures situated far from the designated pumping surfaces are eliminated and the complex structures between divertor and sub-divertor volume are replaced by semi-transparent surfaces. Although the more complex (and thus more realistic) geometry could be used for the simulations at moderate P_{SOL}, at higher power and higher deuterium puffing, the resulting higher neutral pressures in the sub-divertor require significantly more computational resources to calculate the Monte-Carlo neutral trajectories. As a consequence, the higher fidelity geometry was used only for the low (P_{SOL} = 11 MW) power study, with the simplified geometry being adopted for all the higher power (P_{SOL} = 16 MW) runs described in Section "Modelling results for high input power". At moderate power, tests showed that the simplified model gave results within 10% in terms of divertor target profiles of ion flux and electron temperature as obtained with the more complex geometry.

A net plasma flow of 1.5×10^{21} *ions/s* is imposed across the inner core boundary of the simulation, mimicking source from neutral beam injection (NBI), the main additional heating. The P_{SOL} = 11 MW input power to the grid is equally distributed between ions and electrons (note that although the input powers are referred to here as P_{SOL}, in the simulations it is actually the power injected into the inner core boundary

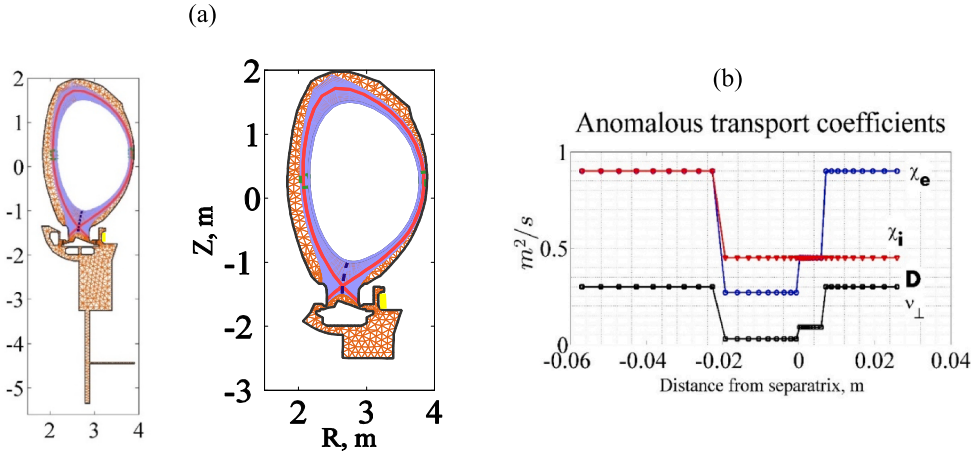

Fig. 1. (a) Modeling geometry including plasma fluid and neutral numerical grids. Pumping surface is marked yellow. (b) Anomalous transport coefficients at the omp.

of the numerical grid, which includes the pedestal region). Deuterium puffing at the rate of 1.7x10^{22} *atoms/s* is introduced in the private flux region (PFR) along with trace impurity (N or Ne) at 10^{17} *atoms/s*. An average plasma toroidal, co-current rotation velocity of 20 *km/s* is imposed at the inner core boundary to reproduce the spin-up induced by neutral beam injection, the principal heating method used in the JET experiments. In the usual way, pumping was simulated by imposing an albedo coefficient < 1 at the pumping surface, Fig. 1(a).

The profiles of transport coefficients at the outer midplane (omp) are shown in Fig. 1(b). They are chosen to try and approximately match the experimentally measured profiles in Fig. 2 of plasma electron density (n_e), electron temperature (T_e) and ion temperature (T_i) for the chosen JET pulse. In the usual way, the extent to which the code reproduces the downstream (divertor target) profiles is then used as a benchmark of the physics model in the simulation. The profiles at both inner and outer targets (experiment and model) for the plate ion saturation current, J_{sat} (a direct measure of the incident charged particle flux) and T_e are given in Fig. 3. Measurements are made with arrays of Langmuir probes. Note that the saturation current to the plate is calculated as "parallel to the magnetic field". This means that the probe current is divided by the perpendicular cross-section of the flux tubes terminating on the probes. Moreover, it is also well known that the T_e measured by such probes in detached divertor conditions is often unreliable, with the probe temperatures recording much higher values than modelling indicates, possibly due to a preferential measurement of the electron tail by the Langmuir probes [11]. This can also explain the inconsistency of measurement and modelling for the PFR region of the outer target, where modelling shows low T_e.

Experimentally the importance of drift flows in JET was shown using discharges with reversed magnetic field [7]. Changing toroidal field direction changes direction of all drift flows. In experiment, changing the magnetic field leads to ceasing of poloidal flows through the SOL and to more symmetric distribution of energy flows to divertor plates. In present modeling the role of drifts in the formation of the divertor parameters was investigated by comparison of full drift runs with calculations without drifts. Turning off drifts whilst conserving all other modelling parameters has little impact on the upstream profiles (Fig. 2) but strongly affects the target profiles (Fig. 3). Both outer and inner target ion currents increase in the absence of drifts, taking the simulated profiles generally far from experiment. Drift induced plasma transport from the ionization zone in the outer divertor through PFR disappears when drifts are deactivated, leading to an increase of plasma flow towards the outer target and a decrease in target T_e. Without this plasma influx from the PFR, the inner target detachment degree decreases and J_{sat} increases.

The relative importance of drift flows can be analyzed using integral parameters, as performed in [2] for ITER and in [12] for AUG. When drifts are activated, the total ionization in the outer and inner divertor plasma regions are 3.8×10^{23} s^{-1} and 4.8×10^{23} s^{-1} respectively, to be compared with 6.3×10^{23} s^{-1} and 5.4×10^{23} s^{-1} with drifts switched off. The flow of ions through the PFR is provided mainly by drifts and reaches a value of 1.5×10^{23} s^{-1}. Parallel flow from the outer to the inner target without drifts is an order of magnitude smaller. The total recombination in the inner divertor with drifts is 3.4×10^{23} s^{-1}, an order of magnitude higher than with drifts switched off, and is comparable to the total ionization. This simple analysis demonstrates that drift flows are not dominant in the divertor region, but can nevertheless strongly impact the solution. In AUG, drift flows are comparable to ionization in the inner divertor [12], whilst in ITER they are an order of magnitude smaller than ionization [2]. The JET case modelled here is thus situated in between.

The marked influence of drifts in the JET case is associated with a nonlinear response of plasma to the particle redistribution between the divertors. The additional flow into the inner divertor from the PFR triggers the onset of volume recombination and subsequent full inner target detachment. The formation of a high field side high density region (HFSHD) [13] follows, as seen clearly in the 2D maps of divertor ionization source, n_e and T_e in Fig. 4. The role of drifts in the formation of this HFSHD feature has been discussed for AUG in [12,14]. The difference seen in the modeling between AUG and JET with regard to this HFSHD is a hot plasma layer separating the X-point region from the cold front. This region is actually even more pronounced in ITER modeling [15].

The role of the $\vec{E} \times \vec{B}$ drift in the formation of the HFSHD region is not only redistribution of particles between the divertors but also changing shape of dense and cold region in front of inner target. $\vec{E} \times \vec{B}$ drift transports plasma from inner strike point vicinity to far SOL along the target plate thus forming the far SOL part of HFSHD region. In this JET case, the radial $\vec{E} \times \vec{B}$ drift flow integrated poloidally in the inner divertor increases by a factor of 3 from 10^{23} s^{-1} at the separatrix to $3{\cdot}10^{23}$ s^{-1} at the flux surface 6 mm at the omp (or 5 cm from the strike point along the inner target). This flow exists for 20–25 cm along the plate, gradually decreasing due to the sink of plasma by both volume and target recombination. The ratio of electrostatic potential to electron temperature, Fig. 5(a), in the HFSHD region indicates that the electric field is determined there by currents under the condition of low electric conductivity, rather than by T_e and pressure gradients [2,12]. The radial electric field at the omp is close to the neoclassical prediction, Fig. 5(b).

The inclusion of drifts into the modeling is essential if the experiment is to be reasonably approximated. Modelled divertor target ion fluxes considerably exceed the measured values (Fig. 3(a,b)) if drifts are switched off. To see if the modelled and measured ion fluxes could be brought closer together in the absence of drifts, a divertor neutral

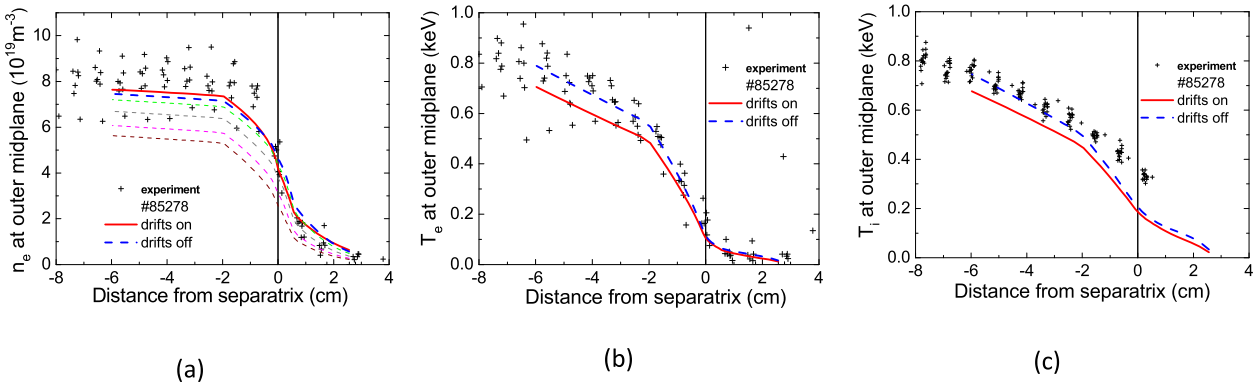

Fig. 2. Plasma profiles at the omp for JET pulse #85278, $P_{SOL} = 11$ MW. a) n_e, b) T_e, c) T_i. Lines are the SOLPS-ITER modelled profiles in each case for drifts switched on (full lines) and off (dashed lines). In (a), the family of dashed lines corresponds to a series of runs without drifts and different pumping strength (see text). In each of the plots, the blue and red lines are always for the same (default) pumping.

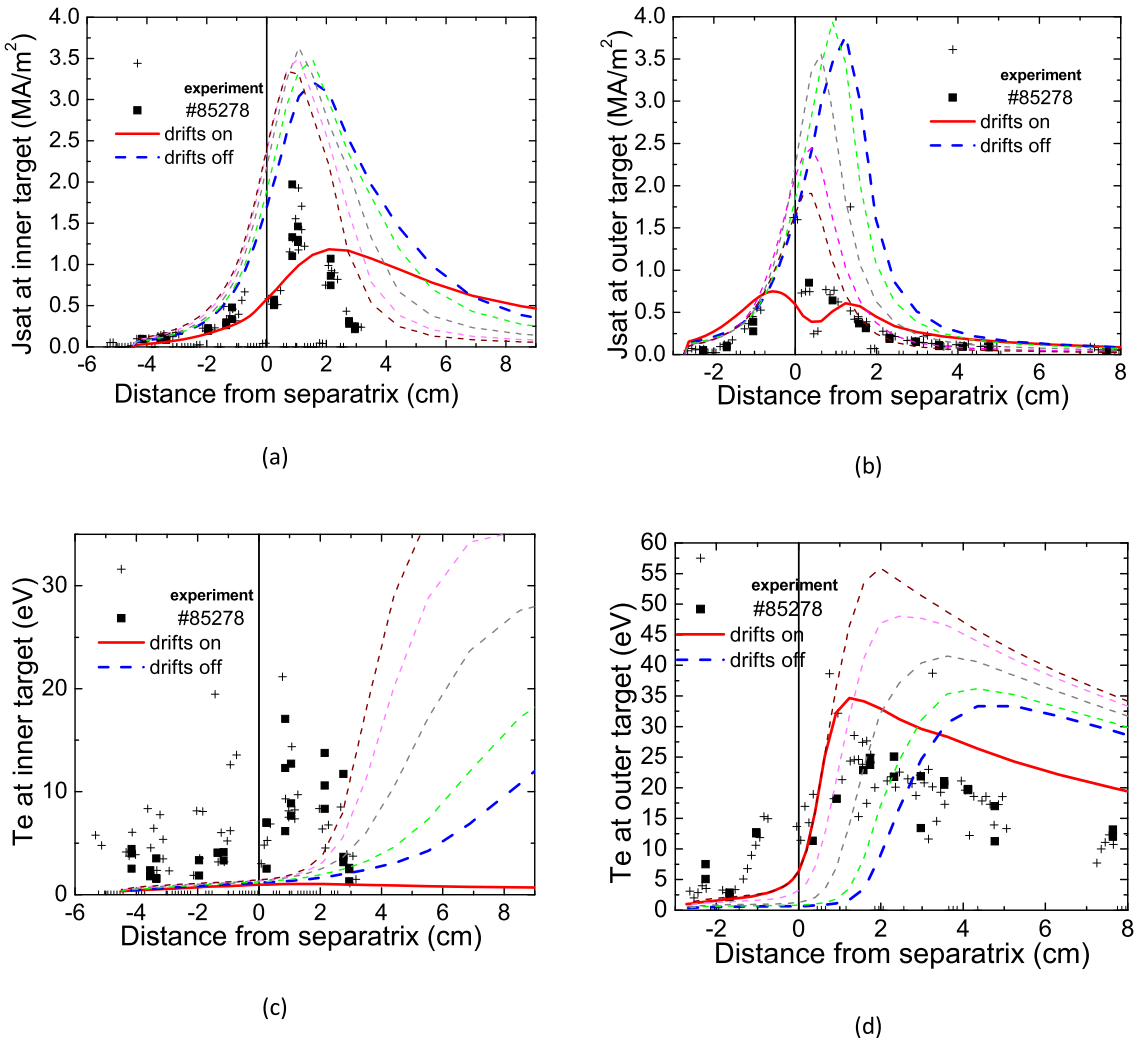

Fig. 3. Divertor target profiles (symbols) of J_{sat} (a,b) and T_e (c,d) at the inner and outer divertor targets for JET pulse #85278, $P_{SOL} = 11$ MW. Lines are the SOLPS-ITER modelled profiles in each case for drifts switched on (full lines) and off (dashed lines). The families of dashed curves correspond to a series of runs without drifts and different pumping strength (see text). In each of the plots, the blue and red lines are always for the same (default) pumping. Note that all experimental data are selected from inter-ELM periods.

pressure scan was performed (drifts switched off) by adjusting the albedo coefficient at the pumping surfaces under the divertor (Fig. 1) to change the pumping efficiency. Increasing pumping in this way, the simulated ion fluxes could be reduced by a factor 2 (and are thus still a factor of 2 higher than the measured values), but at the expense of an increase in the omp separatrix density and a deviation of the upstream density profile from the Thomson scattering measurements.

One noticeable consequence of activating drifts in the model is the double peaked profile found in the outer target particle flux (Fig. 3b). The feature disappears when drifts are switched off. This structure is associated with poloidal $\vec{E} \times \vec{B}$ flow away from the target. The electrostatic potential in the plasma before the target is determined by the sheath condition $\varphi \sim 3T_e/e$. The steep temperature rise from the strike point towards the far SOL (Fig. 3(d)) gives rise to a radial electric field in the range 10–15 kV/m and to a drift velocity $\sim$ 3–5 km/s. This velocity is of the order of the poloidal sound speed (sound speed multiplied by the field line pitch angle). The plasma drag from the target by this drift leads to depletion of the flux tubes where the drift exists and a local decrease of plasma density and ion flux. From a mathematical point of view, since the boundary condition of poloidal velocity equal to poloidal sound speed holds, to compensate the drift, the parallel velocity towards target should increase. For this to occur, the pressure gradient should increase and the pressure in front of the target drops. No such pressure minimum is seen in the experimental saturation current profiles.

One possible explanation for the absence of the structure in experiment could be that increased cross-field transport in the divertor region (i.e. higher than the prescribed values in the main SOL, assumed poloidally constant in the code runs) might "fill in" the density minimum and smear out the temperature front, decreasing the drift velocity. To simulate this, an additional code run was performed with transport coefficients increased by a factor 4 in both divertor regions and in the PFR. As shown in Fig. 6, this does indeed eliminate the double maximum in the ion saturation current profile, at the expense of widening the profile with respect to experiment. Closer agreement with experiment can be recovered by increasing the pumping efficiency. The disappearance of the density minimum is associated mainly with the flattening of the target T_e profile and a resulting decrease of the poloidal drift velocity by factor 2. This exercise proves that further tailoring of the transport coefficients (for example, separate treatment of diffusion and heat conductivity in divertors, etc.) can be used to better adjust the modelling to experiment. However, the baseline agreement between model and experiment is considered satisfactory in terms of providing the basis for predictive simulations of impurity seeding scans at higher P_{SOL}.

Drifts influence also the energy distribution at the divertor entrance. This is illustrated in Fig. 7(a), where only the electron heat conductivity flow can be fitted by an exponential. The characteristic width from the

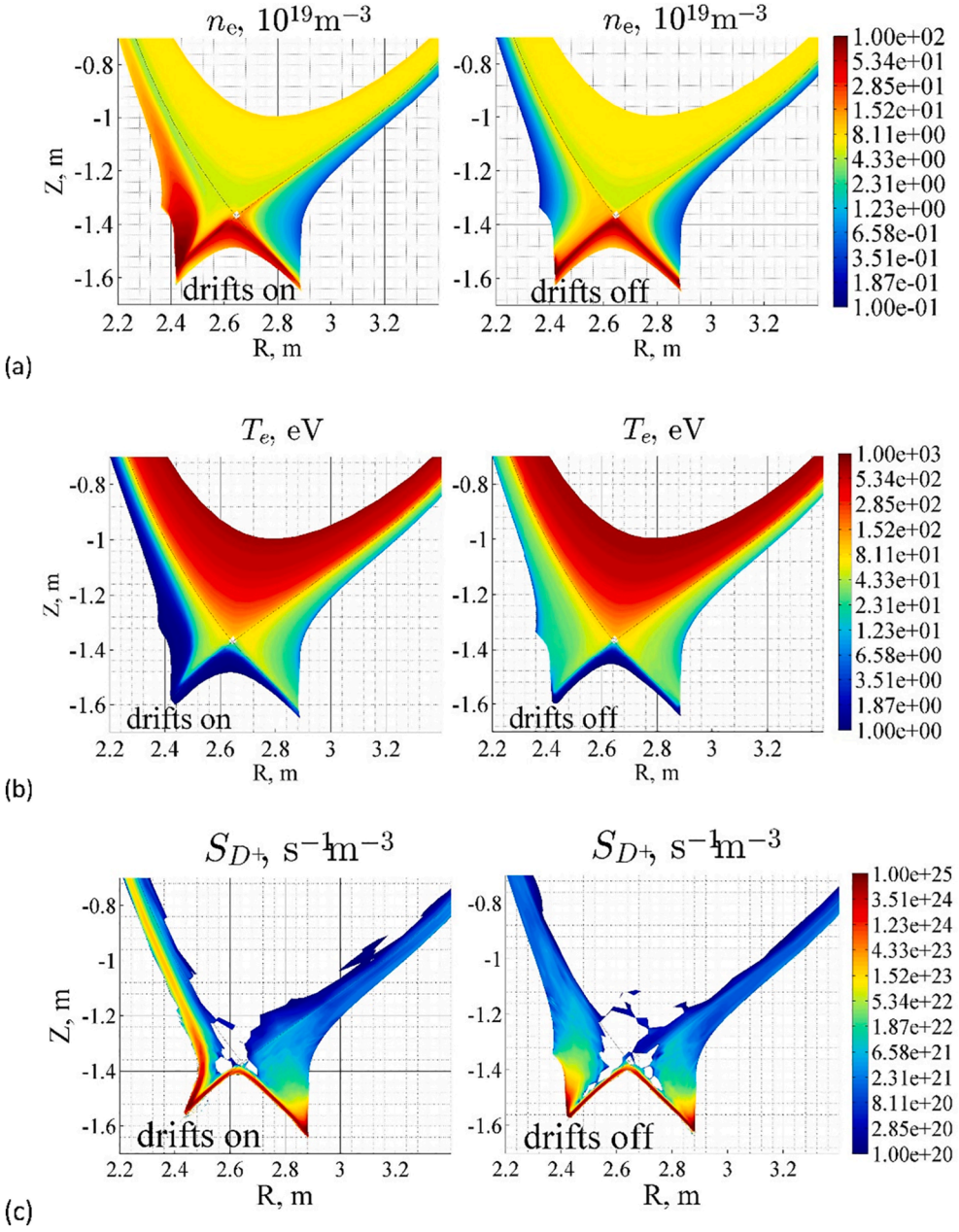

Fig. 4. Simulated distributions with drifts on and off of (a) n_e, (b) T_e, (c) D + ionization source in the divertor region for the benchmark discharge with P_{SOL} = 11 MW.

fit (λ_q) is 2.6 *mm*, agreeing well with characteristic scale length of 9 *mm* for the omp near-SOL T_e obtained in the modeling 2.6 × 7/2 = 9 mm. The full energy flow, including the contributions due to ion and electron convective energy flows is strongly affected by drifts. They are associated with the negative energy flow in the separatrix vicinity, directed here away from the outer target. Moreover the transport of energy through the separatrix from SOL to PFR is affected by radial drifts. The drift contribution here is of the same order as diffusive and radial heat conductivity contributions.

The value of λ_q obtained from the fit to the electron heat flow is a factor ~ 2 higher than would be expected from the empirical Eich scaling [16], itself based partly on data from JET. Since no IR target heat flux data is available for these (vertical target) JET discharges, the only possible comparison between modelled and measured heat flux profiles is to use the target Langmuir probes ($q_{||} = \gamma J_{sat} T_e$, with γ the sheath heat transmission factor). Fig. 7(b) compares the code and experimental outer target profiles for $J_{sat}T_e$, showing quite good agreement between widths of these profiles. The experimental profile maximum is shifted in respect to modeled one due to minimum of modeled J_{sat} profile at the separatrix. Thus, at least for this particular JET discharge, it does appear that the simulated SOL width for electron energy flow is twice as high as expected from the scaling prediction. Note, however, that in the code, λ_q is defined as the characteristic length of the exponential fit to the energy flow at the X-point level recalculated to omp coordinates. In the empirical scaling, λ_q is defined on the basis of a specific simplified expression for the parallel heat flux distribution which cannot be fully justified, so exact coincidence is not necessarily expected.

In this lower power plasma, both Ne and N impurities have been considered, but with low seeding levels such that the impurity does not influence the solution for main plasma component. This trace impurity approach allows the behaviour of the different impurity species to be analyzed on a common background. The absolute values of radiation or

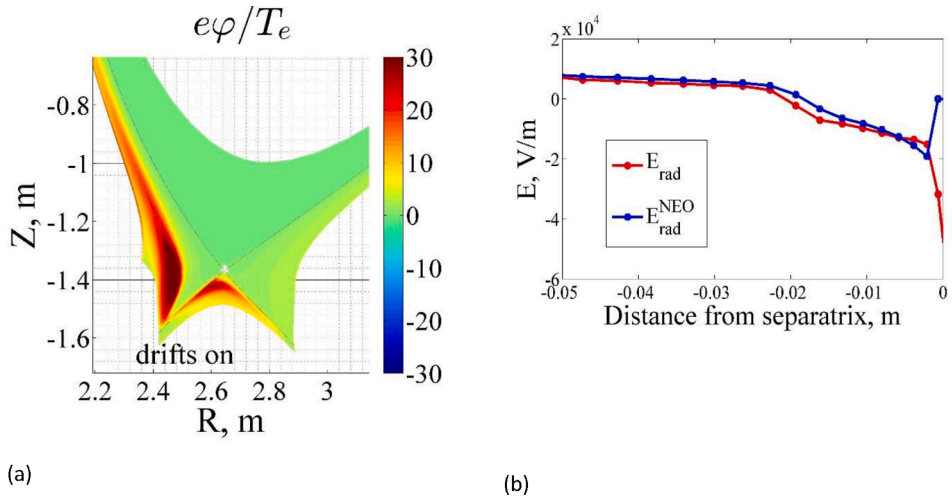

Fig. 5. Simulated electrostatic potential normalized to T_e (a) and radial electric field at the omp (b) for the benchmark discharge with $P_{SOL} = 11$ MW. The radial electric field is compared with the neoclassical value evaluated basing on ions temperature, density and toroidal rotation profiles obtained in the modeling.

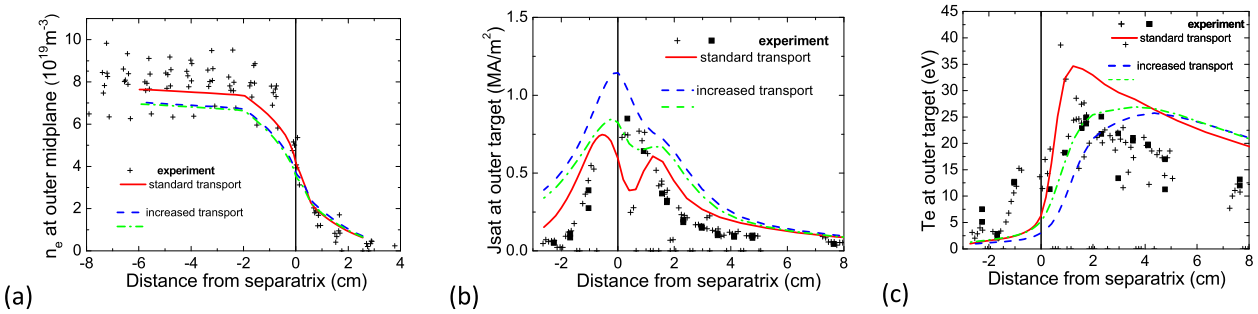

Fig. 6. Comparing the baseline simulation results (red solid lines) with a code run with increased cross-field transport in the divertor (blue dashed lines). The green dashed lines give the profiles for a case with the same enhanced transport, but also with an increase in the pumping strength compared to the baseline. Drifts activated in both cases. (a) upstream n_e; (b) outer target saturation current; (c) electron temperature.

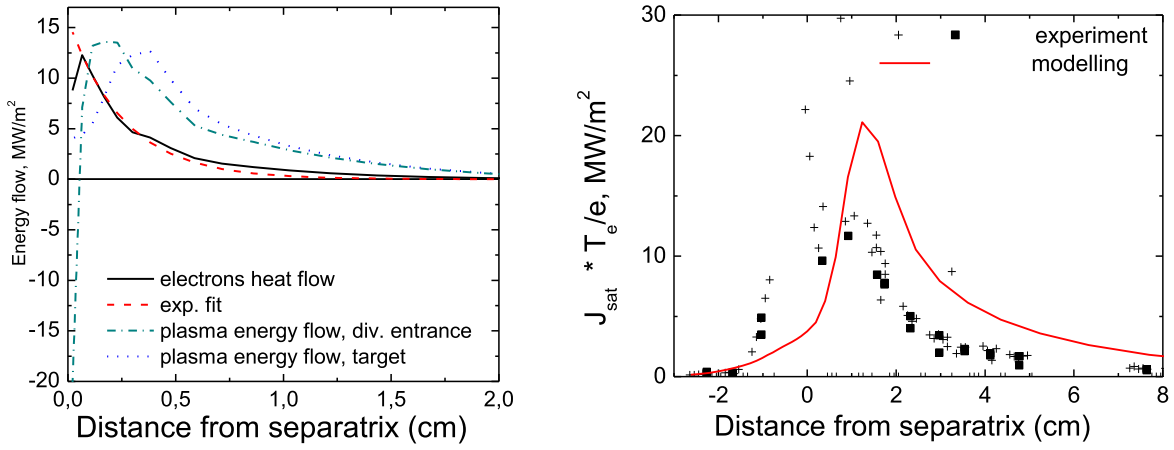

Fig. 7. (a) Energy flows (excluding contribution from neutrals), given divided by the flux tube cross-section at the target and plotted versus distance from the separatrix at the omp. The electron thermal conductivity heat flow at the X-point level is fitted with an exponential with decay length 2.6 mm. Full energy flows at the X-point level and at the target include convective and heat conductivity contributions and the potential energy of ionization. (b) Modelled and measured (using target Langmuir probes) parallel electron heat flux profiles at the outer target.

concentrations are irrelevant since all the impurity features scale linearly with seeding, while the impurity still does not influence the overall solution. Therefore, normalized values are further compared for impurities. As shown in Figs. 8 and 9, N radiation is localized closer to divertor targets due both to better retention of nitrogen in divertor than that of Ne (first ionization potential effect [8]), see Fig. 9, and the dependence of radiation on temperature, see Fig. 8. Nitrogen is fully ionized at lower temperatures so that the maximum of its radiation is

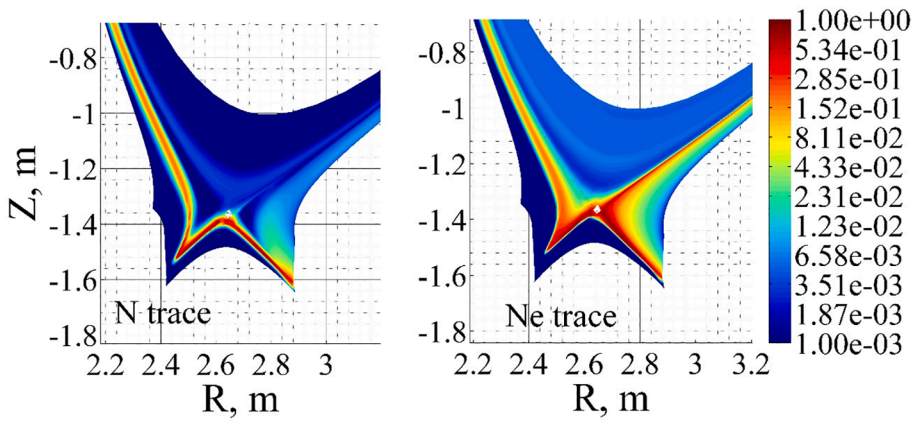

Fig. 8. Radiation per single nucleus for N and Ne, normalized to the peak radiation for each species.

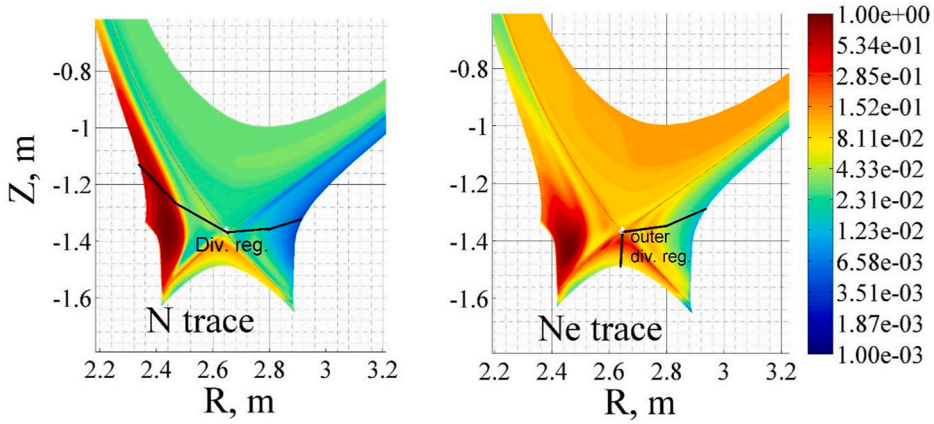

Fig. 9. N and Ne impurity densities normalized to the peak density.

situated at lower temperatures[17,18,19]. The band of high radiation per N nucleus in inner divertor rising towards inner midplane is associated with boundary of cold zone, produced by HFSHD, Fig. 4b. In hotter outer divertor there is no such band. For Ne the zones of high radiation rising towards upstream are present in both divertors. Even though the N radiation is more localized in the divertor than that of Ne, the temperature of the JET pedestal is sufficient to keep the radiation mainly in the SOL and divertor for Ne as well. The radiation per Ne nucleus in the pedestal is <1% of that in the divertor, Fig. 8. The radiation at higher temperature of Ne compared with N makes Ne more suitable for dissipation of energy in the outer divertor before detachment onset.

The distribution of Ne and N density is shown in Fig. 9. Although N is considerably better retained in the HFSHD region at the inner target than Ne, this provides no beneficial effect since the HFSHD region is already highly radiating and well cooled. The main issue is the retention of impurities in the outer divertor, and here N and Ne behave approximately similarly. Comparing the ratio of impurity concentration in the outer divertor SOL (volume averaged; outer divertor region is marked in Fig. 9) to that at the separatrix (surface averaged) gives for 0.8 for Ne and and 1.0 for N. From this starting point it can be foreseen that at least at the beginning of outer strike point detachment (when its temperature drops below 5 eV), Ne should be a more effective radiator than N. For partially-detached regimes, however, Ne can be less well retained than N, as is the case at the inner target.

Modelling results for high input power

Building on the lower input power, trace impurity test simulations described in Section ""Calibration" exercise at moderate input power and trace impurity", predictive modeling of seeding scans with N and Ne at higher power has been performed with $P_{SOL} = 16$ MW imposed at the core boundary of the computational domain, equally distributed between ions and electrons. A fixed deuterium puffing rate of $3.4 \cdot 10^{22} atoms/s$ was chosen as representative of the values expected in these higher power discharges. The geometry of the discharge, the pumping efficiency (albedo) at the sub-divertor structures and the radial transport coefficients were maintained as in the lower power modeling.

The simulated profiles of main parameters at the outer midplane are shown in Fig. 10. Both impurities lead to similar behavior of the omp profiles. As the impurity density increases (increase in impurity throughput), the pedestal density first rises then decreases, with the temperature doing the opposite (as might be expected). The explanation of this behavior is given further. The maximum density in the pedestal in these series is very close to the Greenwald limit. In this predictive modeling the transport coefficients in the pedestal remain unchanged with input power, which may not be the case in experiment. A further reason for the very high pedestal density can be the small separation between the boundary of the plasma mesh and the separatrix at the omp in the modeling. Recombination of plasma at this artificial boundary gives rise to a flow of neutrals. The contribution of this flow to the solution in the SOL is negligible if the SOL density decay length is less than the omp plasma mesh width. However, for regimes with high SOL opacity for neutrals originating from the divertor, this artificial recycling source can significantly affect ionization inside separatrix and can therefore increase the density profile gradient inside the transport barrier.

The companion plots to those in Fig. 10 for the outer divertor target

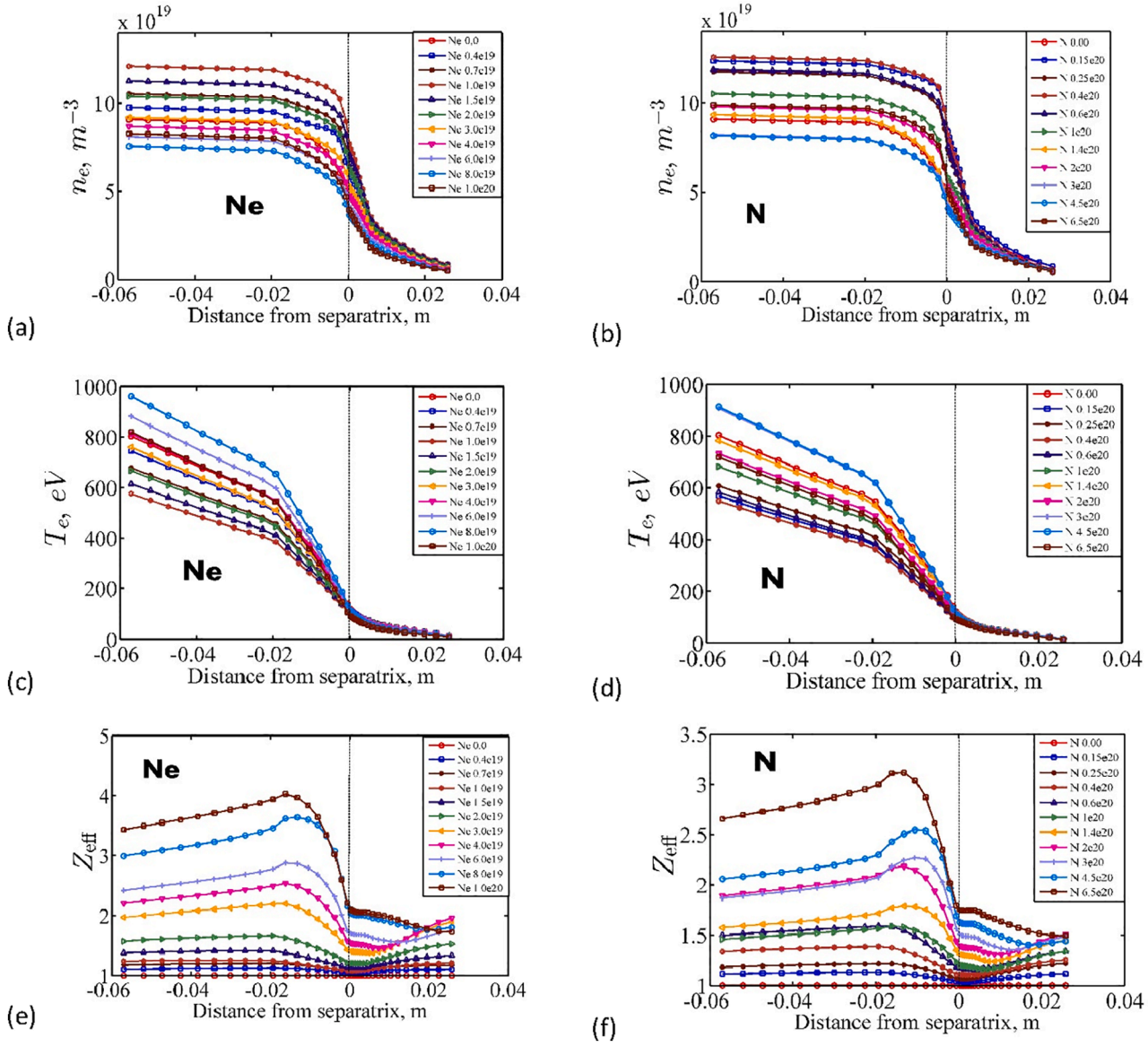

Fig. 10. Modelled parameters at the omp for 16 MW input power: a) electron density, Ne; b) electron density, N; c) electron temperature, Ne; d) electron temperature, N; e) Z_{eff}, Ne; f) Z_{eff}, N.

are shown in Fig. 11. In Fig. 12, some of the key simulation parameters related to the target detachment and upstream density behaviour are graphed against the upstream separatrix impurity concentration for the two seeded species. The initial upstream density rise at the omp corresponds to the outer strike point cooling below 5 eV, outer strike point detachment onset and increase of the modelled saturation current to the outer target, Fig. 12(a). The cooling of the separatrix due to impurity radiation at this initial stage of seeding ramp-up leads to better penetration of deuterium neutrals from the PFR to the SOL. This leads to an increase of ionization in near SOL, an increase of saturation current and therefore to an increase in the upstream pressure. At the same time, the upstream temperature slightly decreases. Finally, the upstream separatrix density increases considerably (see also Fig. 12(b)). Further increase of seeding has the opposite effect. The opacity of the PFR to neutrals stays low, but higher impurity concentrations increase the radiation losses and decrease ionization losses. As a result, the target ion flux and the upstream density decrease.

For both N and Ne, increasing the seeding rate shifts the high temperature front at the outer target towards the far SOL and leads to an ion flux roll-over, Fig. 11(a-d). The outer target strike point detachment, Fig. 11(e-f) occurs at upstream separatrix impurity concentrations higher then 0.4% for Ne and 0.7% for N (Fig. 12b), corresponding to approximately the same Z_{eff} at the separatrix and in the pedestal. At this stage, the heat load decreases from 15 MW/m^2 to <5 MW/m^2 and the target is already protected from excessive localized plasma energy flow. Roll-over demands considerably higher concentrations, approximately the same for Ne and N, leading to higher Z_{eff} in the pedestal for Ne. As illustrated in Fig. 13, a decrease in the particle content of the HFSHD region during the seeding ramp-up is observed in this JET modeling, as seen earlier in AUG modeling and experiment [12,13,14]. Both the spatial dimension and the peak density of the HFSHD region decrease. The process evolves slowly, together with roll over at the outer target with the same upstream separatrix concentrations of Ne and N. The particle content in outer divertor remains almost unchanged during increase of impurity concentration.

The retention of Ne in the divertor is worse than that of N, which is consistent with modeling of both AUG and ITER [15]. This is illustrated in Fig. 14(a). A robust integral measure of impurity retention/leakage can be expressed by the ratio of impurity concentration in the pedestal, or at the upstream separatrix, to impurity seeding relative to deuterium

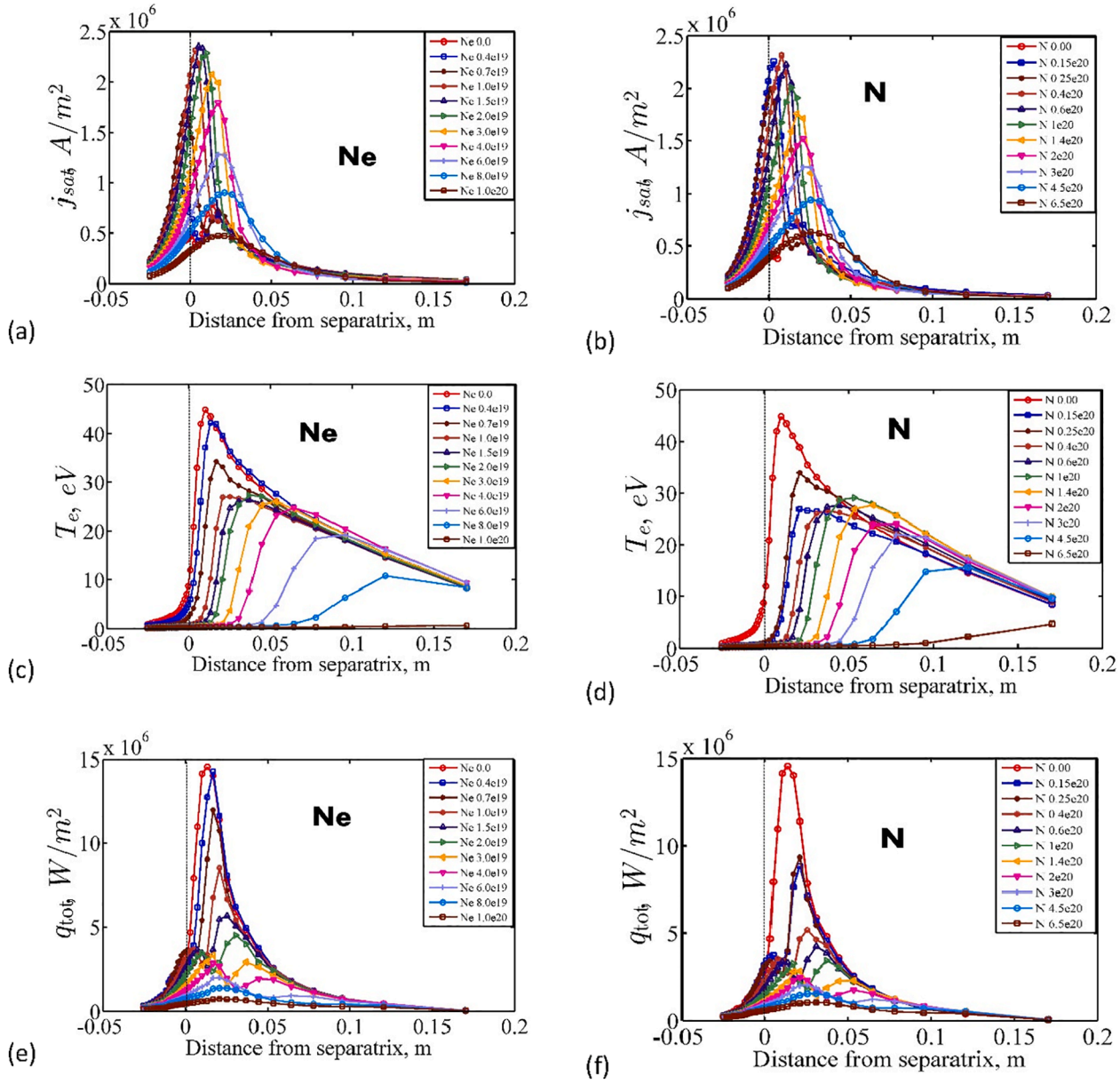

Fig. 11. Modelled parameters at the outer target for 16 MW input power: a) parallel ion saturation current, Ne; b) parallel ion saturation current, N; c) electron temperature, Ne; d) electron temperature, N; e) target heat load, Ne; f) target heat load, N.

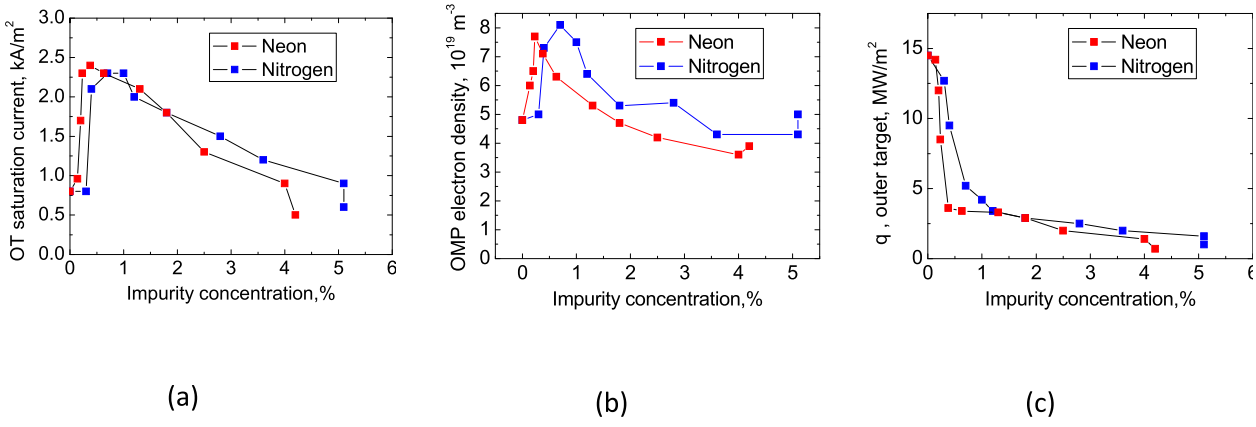

Fig. 12. Selected key simulated parameters as a function of upstream omp separatrix impurity concentration: a) peak parallel outer target ion flux; b) electron density at the omp separatrix; c) peak outer target power flux.

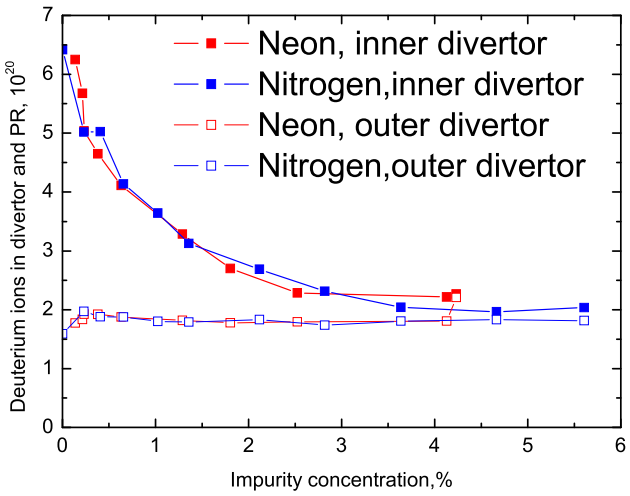

Fig. 13. Total particle content (D molecules, atoms and ions) in the inner and outer divertor as functions of upstream separatrix concentration.

puffing. The latter gives an integral measure of the partial impurity pressure in the sub-divertor structures in front of the pump, while the former is a measure of impurity penetration to the upstream plasma. This is valid if there is no significant difference in loss channel for impurity pumping, which, in experiment, could be different for different impurity species. In the modeling, the deuterium puffing is maintained constant during the seeding scan and impurity is removed only by pumping, so the relative retention can be estimated through the dependence of impurity concentration on the seeding.

From Fig. 14(a), the retention of both impurity species at low seeding (before the outer strike point detachment) is very similar. As the impurity injection increases and target ion flux roll-over begins, N is retained in the divertor about a factor 4 more efficiently than Ne. This may also be seen in Fig. 14(b), where the average concentration of impurity in the outer divertor (the region marked in Fig. 9) is plotted as function of the average concentration at the separatrix. Before the outer strike point detachment, for impurity concentrations below 0.7%, N and Ne behave similarly. For higher concentrations retention of N in outer divertor is considerably better.

In Fig. 15, the normalized N and Ne densities are compared for two pairs of the simulations with approximately the same distributions of outer target ion flux and temperature. For these high power seeded JET runs, the outer divertor retention is comparable for both species before the onset of partial detachment, Fig. 15(a), and then becomes significantly better for N once partial detachment is achieved, Fig. 15(b). It can therefore be expected that N and Ne perform similarly for the attainment of strike point detachment, but that N is better for well developed detachment states.

The distribution of impurity radiation in the divertor for the same pair of runs is shown in Fig. 16. For moderate seeding, the radiation is localized in the divertor for both radiating species, while for higher seeding it remains in the divertor region for N and begins to move upstream for Ne. This behavior is associated with both worse Ne retention and with the tendency for Ne to radiate at higher temperatures than N.

The dependence of retention on degree of detachment can be explained by the first ionization potential (FIP) effect proposed in [8] for AUG and in [15] for ITER. A more pronounced FIP effect for partially-detached plasmas than that in attached regimes at low seeding levels is associated with the specific temperature profile in the partially-detached regime. In each detached flux tube in this regime there is a cold region with temperature well below 5 eV, with almost no ionization, and similar poloidal velocity directed towards the divertor target for both fuel and impurity ions. The boundary of this cold zone is a region with very steep temperature gradient, with temperature rising up to ~100 eV over a poloidal scale length of 10 cm. The ionization front for the main ions is situated in this narrow zone, from where parallel flow towards the plates originates and at the same time here the thermal force begins to act, deviating the impurity velocity from that of main ion component, giving rise to an impurity velocity directed upstream. As a consequence, the impurity ionization potential dramatically influences the retention, determining the exact position of the impurity ionization front within the steep temperature gradient and in the presence of a stagnation point of impurity flow all in the same small region.

In less detached regimes, the FIP effect is still present but less pronounced. The ionization rates dependence on temperature is very steep at temperatures smaller than first ionization potential of atom [20]. When T_e is comparable or bigger than first ionization potentials of all species, the position of ionization depends more on the electron density profile than on temperature distribution. Therefore for attached conditions when T_e is big almost everywhere in the divertor, the impurity ionization position is less sensitive to the first ionization potential and less separated spatially for different species of impurities and main ions. The retention of different sorts of impurities in these regimes is comparable. Also the temperature gradient is less steep in the ionization region and the position of the stagnation point for poloidal impurity flow is determined by several factors, including drifts. This is supported by modeling. For the trace impurity case, Fig. 9, the peak impurity density in the detached inner divertor is much more pronounced for N than for

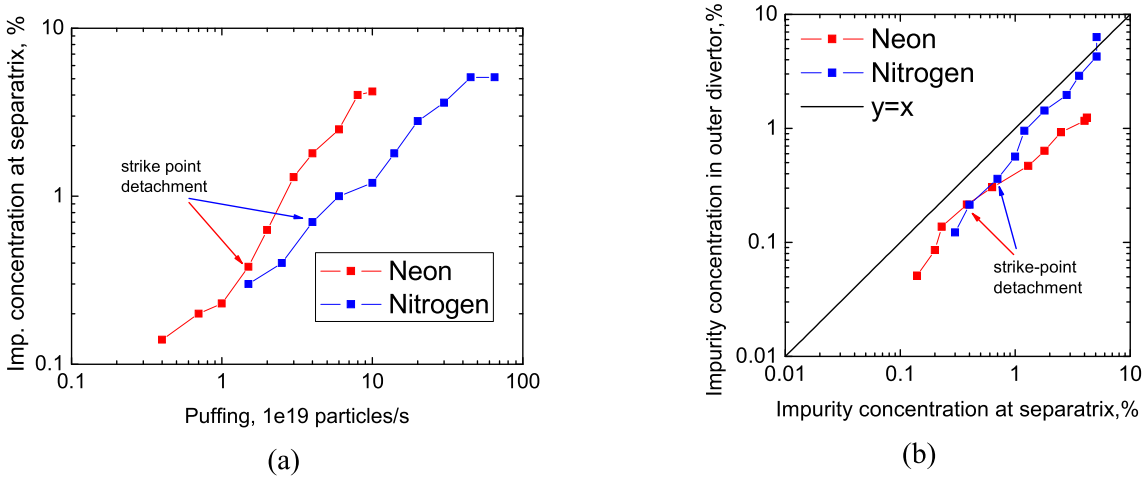

Fig. 14. (a) Surface averaged ionized impurity separatrix concentration as a function of seeding injection rate. (b) Impurity (sum of ions and neutrals) average concentration in the outer divertor plasma volume as a function of upstream impurity separatrix concentration.

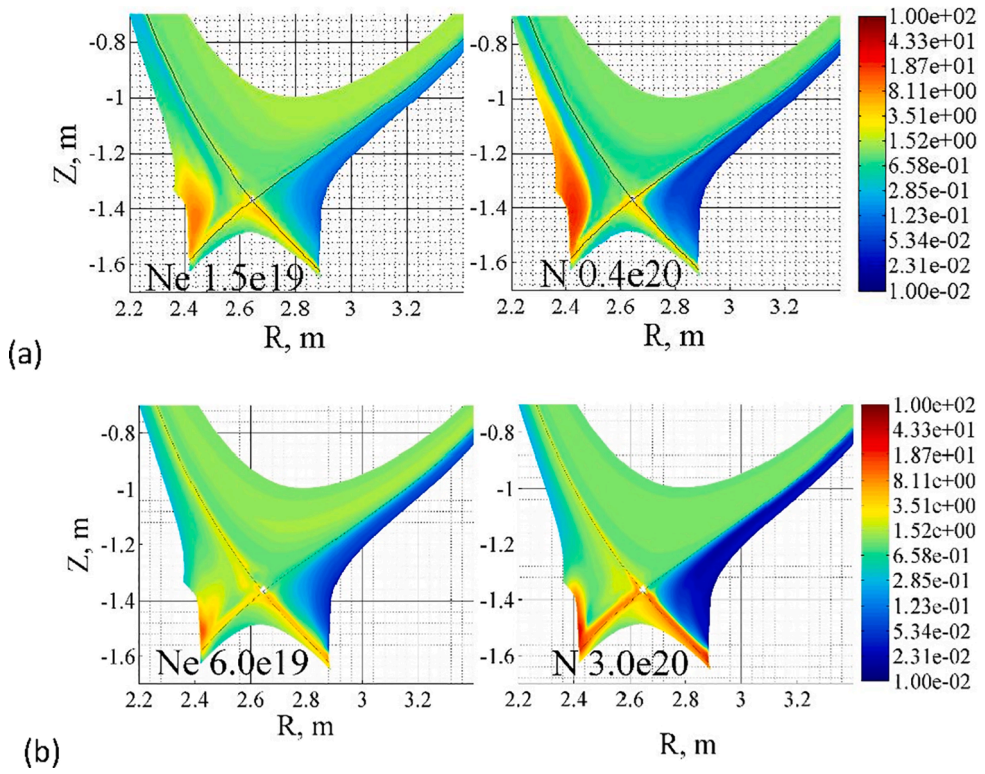

Fig. 15. Impurity density normalized to the volume averaged density (a) moderate seeding, (b) high seeding (Left plots: Ne, right plots: N).

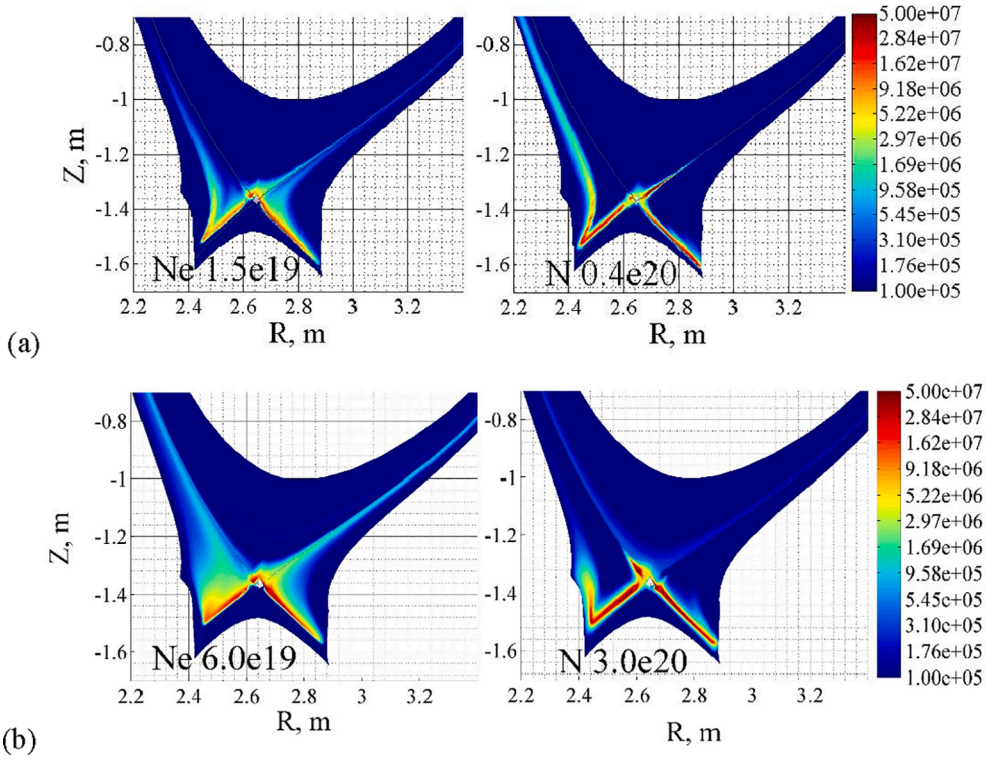

Fig. 16. Impurity radiation (a) moderate seeding, (b) high seeding (Left plots: Ne, right plots: N).

Ne, while the retention of both species in the attached outer divertor is comparable.

As shown in Fig. 17, the fraction of energy radiated in the divertor (inner and outer regions marked in Fig. 9) also supports the statement of similar behavior of both N and Ne at low seeding and considerably better radiation localization in the divertor for N at high radiated power fractions. It is interesting to compare the present modeling results for JET with the SOLPS-ITER simulations in Ref. [15] for AUG and ITER with N and Ne and with modeling results with drifts for wide range of Ne seeding described in Ref. [2]. The simulation points in Table 2 of [15]

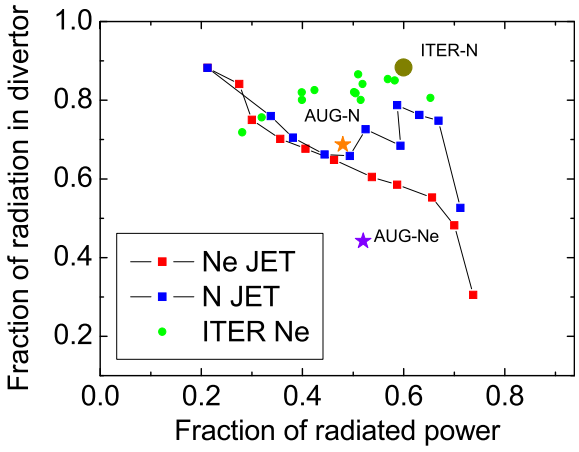

Fig. 17. Ratio of divertor radiation (ions and atoms) to the total radiation in the modeling domain as a function of total radiation normalized to the input power. For comparison, additional points have been added from equivalent modelling studies (including drifts) with SOLPS-ITER for AUG and ITER extracted from [2,15].

and points for runs with drifts described in [2] have been added to the JET cases in Fig. 17, showing how both the Ne and N radiation is localized in the divertor in ITER, even for very high radiated power fractions (see also [1]). For AUG, Ne radiates poorly in the divertor in comparison with N and JET lies somewhere in between the two extremes. Thus, the larger the device, the larger the divertor radiated fraction for Ne, whilst N seeded discharges radiate efficiently in the divertor even for medium sized devices. Note that in all three cases (AUG, JET and ITER), the simulation data in Fig. 17 are for vertical target configurations, allowing for a meaningful comparison.

Conclusions

A comprehensive plasma boundary modelling exercise for JET has been conducted with the SOLPS-ITER code, with fluid drifts activated, to compare the behavior of two ITER candidate medium Z impurity species, nitrogen and neon, foreseen for divertor power dissipation during burning plasma operation. Neon is currently favored for ITER to avoid problems of plasma chemistry (production of tritiated ammonia), but H-mode experiments on AUG have found operation with Ne to be problematic. On JET, N also performs better than Ne, at least for power into the SOL typically accessible until recently. One important contributor to the degraded performance with Ne is thought to be machine scale size, and its impact on divertor retention of impurity. The simulations reported here are an attempt to predict what might be observed at JET when SOL power is increased. Such power levels have in fact recently been obtained and new seeding experiments have been performed. They are not yet, however, fully available for comparison with modelling and so this paper remains as a predictive simulation exercise. Work is underway to compare simulations with the new JET data and the results will be reported in a future publication.

Beginning with a “calibration exercise” in which code runs were performed guided by real experimental data from moderate power, low seeding JET H-mode plasmas, a series of predictive simulations have been made at higher power and with scans of impurity seeding rate for both Ne and N at fixed fuel throughput. For the lower power target discharge, the code satisfactorily reproduces key experimental results both upstream at the outer midplane and at the divertor targets, including the formation of a high field side, high density region seen in experiment. The modeling clearly reveals the importance of drift flows, redistributing plasma between the divertor plates through the private flux region.

For the higher power, seeding rate scans, both impurities are found to produce strike point detachment of the outer target for the same moderate $Z_{eff} < 1.5$ in the pedestal, corresponding respectively to N and Ne concentrations higher than 0.7% and 0.4% at the main chamber separatrix. Significant reductions of the target heat flux are observed already when the ion flux to the outer target is at its peak. Further increase of seeding leads to ion flux roll-over, and to a slow further decrease of the peak target heat load. At this stage, the Ne radiation gradually shifts upstream and finally the fraction of radiation above X-point can reach 50%. In contrast, N radiation is localized mainly below the X-point, until full detachment of outer target.

Comparison of present JET modeling with equivalent SOLPS-ITER simulations of ITER and ASDEX-Upgrade indicates that the localization of radiation in the divertor region depends on machine size. Larger scale size is more favorable for localization of Ne radiation in the divertor, presumably due to higher temperatures at the divertor entrance and higher opacity to impurity neutrals. A more detailed multi-machine simulation exercise for the AUG-JET-ITER triplet is ongoing to further quantify this scale size effect [21].

CRediT authorship contribution statement

Elizaveta Kaveeva: Validation, Formal analysis, Writing - original draft. **Vladimir Rozhansky:** Supervision. **Irina Veselova:** . **Ilya Senichenkov:** Software, Formal analysis. **Carine Giroud:** Investigation. **Richard A. Pitts:** Conceptualization. **Sven Wiesen:** Software. **Serguey Voskoboynikov:** Software.

Declaration of Competing Interest

The authors declare that they have no known competing financial interests or personal relationships that could have appeared to influence the work reported in this paper.

Acknowledgements

This work was supported by Russian Science Foundation, grant no. 20-52-53025 and conducted partially under the auspices of the ITER Scientist Fellow Network. Numerical calculations were performed at the Polytechnic Supercomputer Center at Peter the Great St. Petersburg Polytechnic University. The views and opinions expressed herein do not necessarily reflect those of the ITER Organization. This work has been carried out within the framework of the EUROfusion Consortium and has received funding from the Euratom research and training programme 2014-2018 and 2019-2020 under grant agreement No 633053. The views and opinions expressed herein do not necessarily reflect those of the European Commission.

References

[1] R.A. Pitts, et al., Nuclear Mater. Energy 20 (2019), 100696.
[2] E. Kaveeva, et al., Nucl. Fusion 60 (2020), 046019.
[3] C. Giroud, et al., Towards Baseline Operation Integrating ITER-relevant Core and Edge Plasma within the Constraint of the ITER-Like Wall at JET. presented at IAEA 25th Fusion Energy Conference (FEC 2014) Saint-Petersburg, Russia, 2014.
[4] M. Bernert, et al., Nucl. Mater. Energy 12 (2017) 111.
[5] L. Casali, et al., Phys. Plasmas 27 (2020), 062506.
[6] A.E. Jaervinen, et al., J. Nucl. Mater. 463 (2015) 135–142.
[7] R.A. Pitts, et al., J. Nucl. Mater. 337–339 (2005) 146–153.
[8] I.Y. Senichenkov, et al., Plasma Phys. Control. Fusion 61 (2019), 045013.
[9] C. Giroud, et al., Plasma Phys. Control. Fusion 57 (2015), 035004.
[10] S. Wiesen, et al., Nucl. Mater. Energy 17 (2018) 1.
[11] J. Watkins, et al., J. Nucl. Mater. 241–243 (1997) 645.
[12] V. Rozhansky, et al., Contrib. Plasma Phys. 58 (2018) 540.
[13] S. Potzel, et al., J. Nucl. Mater. 463 (2015) 541.
[14] F. Reimold, et al., Nucl. Mater. Energy 12 (2017) 193.
[15] E. Sytova, et al., Nucl. Mater. Energy 19 (2019) 72.
[16] T. Eich, et al., Nucl. Fusion 53 (2013), 093031.
[17] A. Kallenbach, et al., Plasma Phys. Control. Fusion 55 (2013), 124041.
[18] C. Giroud, et al., Plasma Phys. Control. Fusion 57 (2015) 3.

[19] L. Casali, et al., Phys. Plasmas 25 (2018), 032506.
[20] P.C. Stangeby, The Plasma Boundary of Magnetic Fusion Devices, in: P.C Stangeby (Ed.), Institute of Physics Pub., Bristol; Philadelphia, 2000Print.
[21] V. Rozhansky et al., "Multi-machine SOLPS-ITER comparison of impurity seeded H-mode radiative divertor regimes with metal walls" accepted for presentation at the 28th IAEA Fusion Energy Conference (FEC 2020) Nice, France 10-15 May 2021.